Efficient, reliable, long-lifetime, diode-pumped Nd:YAG laser for space-based vegetation topographical altimetry

Donald B. Coyle, Richard B. Kay, Paul R. Stysley, and Demetrios Poulios

A highly efficient, diode-pumped, Nd:YAG laser is described. The oscillator utilizes an unstable resonator design with a Gaussian reflectivity output coupler and a side-pumped zigzag slab gain medium. The laser produces 18-mJ, 10-ns pulses at a repetition rate of 242 Hz in a near-TEM_{00} mode with an optical efficiency of up to 14%. An extended performance test was recently concluded in which the transmitter operated at reduced output for more than 4.8×10^9 shots with no optical damage. Design criteria, beam quality, and lifetime data are presented. © 2004 Optical Society of America

OCIS codes: 280.3640, 140.3540, 140.3580, 140.5560, 140.6810, 140.3480.

1. Introduction

We report on a high efficiency laser, originally designed as a prototype transmitter for a National Aeronautics and Space Administration space-based lidar mission for topographical measurements of the earth, similar to the Vegetation Conopylidar (VCL) and Geoscience Laser Altimeter System missions.[1,2] Data products for such missions require that the laser wave form be nearly pure Gaussian, both temporally and spatially, with a uniform phase front. A single spatial mode insures that no other "hot spots" other than the central lobe will be present in the 25–100-m-diameter ground footprints, and the digitized time of flight waveform returns provide the topographical structure.[3] We first describe the laser architecture, including details of the unstable resonator and the pump head. Although much of the system design is standard engineering practice, certain innovative elements are implemented that are unique to this laser. Considerable effort in this design was geared toward maximizing system reliability and efficiency. In particular, great care has been taken to ensure that this design could successfully operate up to two years in space with no self-induced optical damage. In the VCL project, for example, approximately 2.3×10^9 pulses per year are required. For damage-free operation in a harsh, hands-off, environment such as space, a major form of damage risk reduction is the creation of a large intracavity mode to reduce the peak fluence. The intracavity mode, however, must also be small enough to ensure good optical efficiency, requiring a somewhat delicate balancing act between the two factors. High efficiency is key to future laser-based space missions for reduced total cost and improved total system reliability and stability. Higher efficiency allows reductions in instrument size, mass, solar array area, drive and support electronics, and heat removal requirements. Since wallplug efficiencies of diode-pumped Nd:YAG systems are typically below 5%, at best, even a 1% or 2% improvement is a relatively huge gain. Additional requirements placed on the laser include compactness, ruggedness, tolerance of moderate temperature variations, and good shot-to-shot pointing stability.

2. Oscillator Architecture

A three-dimensional engineering drawing of the High-Efficiency Laser Transmitter (HELT) is presented in Fig. 1. The conductively cooled laser features an optically efficient pump head incorporated in a concave–convex unstable resonator with a graded reflectivity mirror (GRM) output coupler. The zigzag slab had near-Brewster end faces, and was side pumped (x axis) with seven four-bar stacks of Spectra Diode Labs back-cooled, diode arrays, rated at 60 W per bar. These diodes were selected to have ~49% electrical-to-optical efficiency upon procurement and were typically operated de-rated by ~17% below the

D. B. Coyle (barry@cornfed.gsfc.nasa.gov) is with the National Aeronautics and Space Administration Goddard Space Flight Center, Code 920, Greenbelt, Maryland 20771. R. B. Kay, P. R. Stysley, and D. Poulios are with the Department of Physics, American University, Washington, D.C. 20016.

Received 13 February 2004; revised manuscript received 16 June 2004; accepted 21 June 2004.

0003-6935/04/275236-07$15.00/0

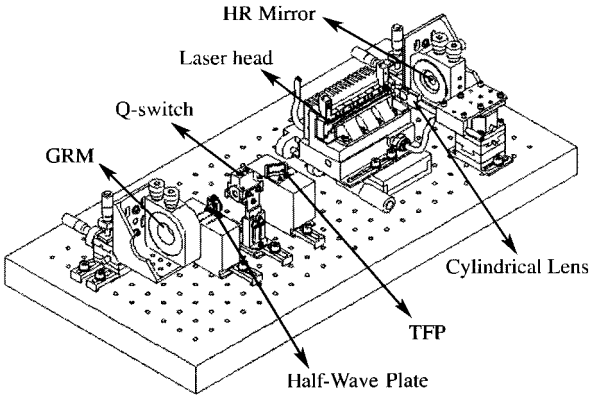

Fig. 1. The HELT configuration. It was important to have modularity and micrometer motion control on the head and end mirrors for thorough performance characterization.

peak output power in order to extend their operational lifetime. The zigzag slab geometry cancels optical distortion in one axis to the first order, and side pumping takes advantage of the natural geometry of the multistripe diode array, allowing efficient coupling of the pump energy into the intraslab mode volume.[4,5] The slab has a center length of 95 mm along its optical z axis and was 2.65 mm thick (x axis) and 5 mm wide (y axis). The laser has some similarities to the 100-mJ high-brightness design of Armandillo *et al.*,[6] which was also a side-pumped slab laser employing an unstable resonator. The obvious differences between our design and that of Armandillo *et al.* are in output energy and laser head pumping geometry. Additionally, there are more subtle differences, such as our use of an even-bounce slab, a stepped heat sink for reduction of thermal lens, a shorter resonator for space conservation, and a large margin of overhead in pump-diode power. Other diode side-pumped slab designs that have gone into space have not employed an unstable resonator but rather used porro or retro prisms as end mirrors for their expected high alignment stability and large multimode beam production.[7,8]

3. Slab Details

Since high efficiency was critical to this laser's possible use as a space-based transmitter, it was decided to revisit some established solid-state laser development tools in detail such as zigzag slab design and pump-volume mode matching. An even-bounce parallelogram design was used that is less subjected to end-mirror pointing errors than an odd-bounce (trapezoid) design. An even-bounce slab has entrance and exit window faces that are parallel, so that if the entrance beam deviates upward the output beam deviates upward at the same angle. A ray entering an odd-bounce slab that is not parallel to the z axis will exit the slab at an equal but opposite angle. Thus odd-bounce zigzag slabs exacerbate mechanical sensitivity.

In order to provide maximum gain overlap or "fill" of the pump beam with the elliptical intraslab mode, we set our slab's tip angle to 26.5°. The x axis of the laser mode, parallel to the zigzag plane, is increased in the slab by refraction at the end faces. It can be easily shown that the x axis of the intraslab mode (ω_x) is related to the tip angle and the incident x axis external mode (ω_o) by

$$\omega_x = \omega_o \frac{\cos(\alpha)}{\sin(\varphi)}, \tag{1}$$

where φ is the tip angle and α is the refraction angle obtained from Snell's law. Brewster's angle for Nd:YAG at 1.064 μm is $\theta_B = 61.2°$ and $\omega_x/\omega_o = 1.82$. For a tip angle of 26.5°, as used in our design, this ratio increases to 1.95, increasing the x axis diameter of the intraslab beam by ~7%. Since the slab face is near Brewster's angle, the polarized beam loses very little energy owing to reflection. The slab is pumped along the x axis with one of the faces high-reflection (HR) coated so that the light is double passed through the slab. This yields a calculated absorption of ~93% when an in-house measurement of absorption cross section of $\sigma_{abs} = 3.4 \times 10^{-20}$ cm^2 is used for 1.1% doped Nd:YAG.[9] This effective cross section includes the overlap of the pump-diode spectral width with the Nd:YAG absorption feature between 805 and 812 nm; this was measured by temperature tuning a collimated diode laser to maximum absorption through 1.1% Nd:YAG. Comparison with published absorption data that does not include this overlap is difficult. Spectra typically presented are at relatively low resolution.[10,11] However, the 1% Nd:YAG absorption spectra of Zhou *et al.*[12] has sufficiently high resolution to be useful. Most importantly, Zhou *et al.* also showed the absorption coefficient of the GaAlAs laser diode passing through the bulk 1% doped Nd:YAG as the center wavelength of the diode is temperature tuned through the absorption peak. The maximum value from their Fig. 2 is α ~4.55 mm^{-1}. This converts to an effective absorption cross section of $\sigma_{abs} = \alpha/\rho = 3.3 \times 10^{-20}$ cm^2 by use of $\rho = 1.38 \times 10^{20}$ cm^{-3} for 1% doping and is in excellent agreement with our value.

The intracavity beam $1/e^2$ diameter was designed to be ~2 mm. The thickness of the slab therefore should not greatly exceed this, or the zigzag beam path will miss large regions of the pumped volume and not sweep out the stored energy efficiently. We discovered inherent aperture effects created by use of an angle of incidence less than Brewster's angle for the x axis and subtle effects on the beam's y axis from varying pump beam thickness. Depending upon the chosen slab tip angle, the rays that enter the slab nearest to the tip were refracted such that upon their second internal total internal reflection they strike the inside of the slab entrance face rather than the opposing zigzag surface. Such rays were deviated from the normal zigzag pattern and did not contribute to the cavity mode. For our chosen tip angle of 26.5°, the full width of the slab's acceptance aperture was 2 mm. In combination with our final pump beam design, the 26.5° tip was very useful in main-

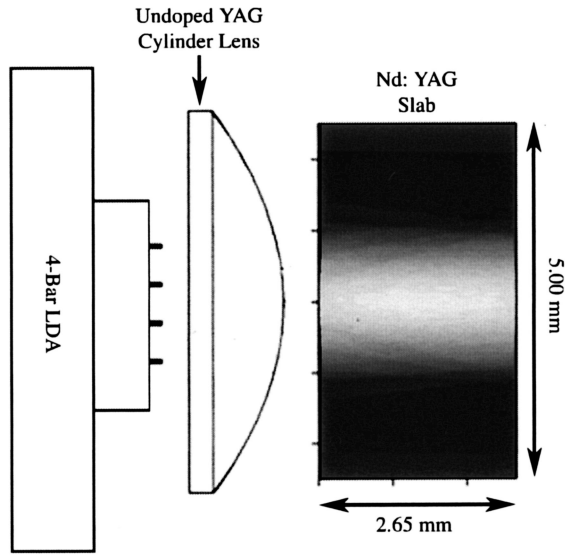

Fig. 2. Modeled distribution of pump radiation in slab. The four-bar diode array and undoped cylindrical lens produces a relatively smooth absorption distribution in the Nd:YAG slab, as seen on the right side of the figure.

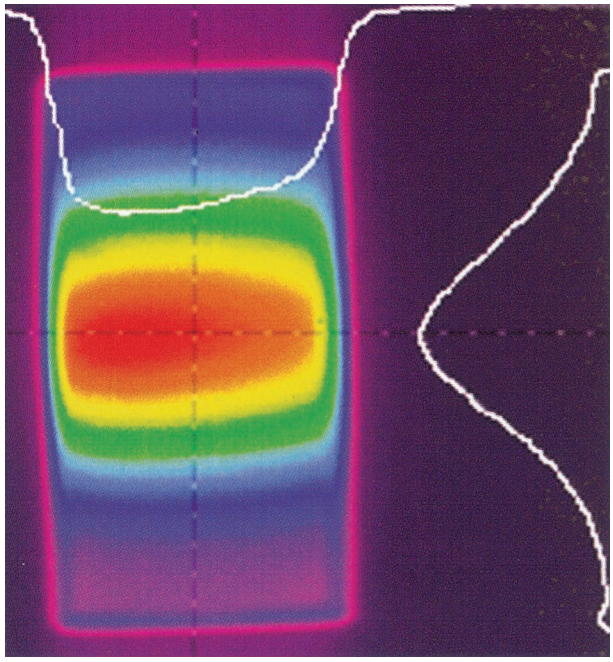

Fig. 3. A CCD image of the 1064-nm fluorescence emanating from the end of a rectangular Nd:YAG slab when pumped in the HELT head configuration. The diode energy enters from the left and is reflected off the right slab face for a two-pass pump path.

taining a single spatial mode while retaining high-energy extraction efficiency.

4. Collimated Pump Beam

Since resonator efficiency depends strongly on the inversion density of the gain medium, it is advantageous to confine the pump light in the transverse dimension such that it matches the desired cavity mode as closely as possible. To accomplish this, the 809-nm light from the diode arrays was collimated in the fast axis by a single plano-convex cylindrical lens made of undoped YAG. The resulting transverse pump light distribution from the diode-lens-slab optical system was then modeled with a commercial raytracing software package and is shown in Fig. 2.

This pumping scheme can be contrasted with close-coupled side-pumping results in which the diode-array 809-nm radiation fills the active medium and a weaker thermal lens results. However, such pumping schemes are unsuited for highly efficient 10–20 mJ oscillator designs operating in a near-TEM_{00} mode. Lensed designs can enhance optical efficiency by creating an intense stripe of pump energy down the slab length, maximizing the inversion density and cavity mode overlap with the pumped region.

Care was taken when positioning the lens relative to the diode arrays, as the pulse energy and beam quality are sensitive to this adjustment. If the pump lens was placed too far from the diode facets, the pump beam would focus inside the slab, creating a strong thermal lens as well as a number of undesirable "hot spots" in the gain medium. Similarly, if the lens was too close to the arrays, the pump beam would be too divergent, creating a larger pump volume and reducing the optical efficiency of the resonator. When the pump lens was optimally situated, the collimated pump beam closely approximated a Gaussian distribution in the vertical dimension with a $1/e^2$ radius of $\sim$1.4 mm inside the slab. The Gaussian nature of the pump light distribution can be seen in an image of 1064-nm fluorescence emitted from the slab end in Fig. 3. The ability to precisely adjust both the pump lens-diode array distance and the slab-diode array to $+/-0.125$ mm was incorporated into the head design. Figures 4 and 5 show the laser head and a cross section of the final assembly.

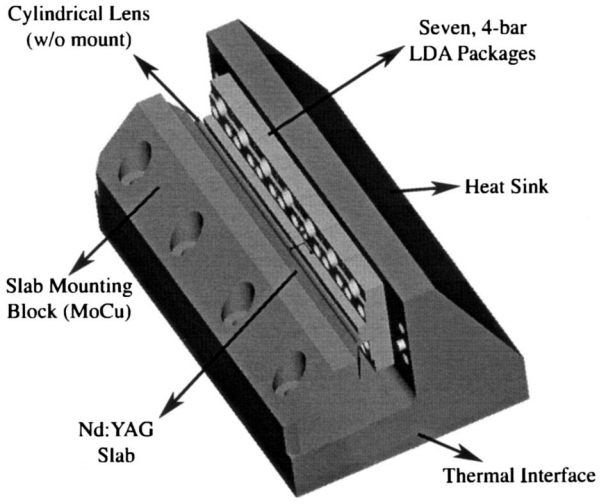

Fig. 4. Pump head configuration (the pump lens mount is not shown). The Nd:YAG slab is thermally bonded to a molybdenum copper block in order to match thermal expansion coefficients.

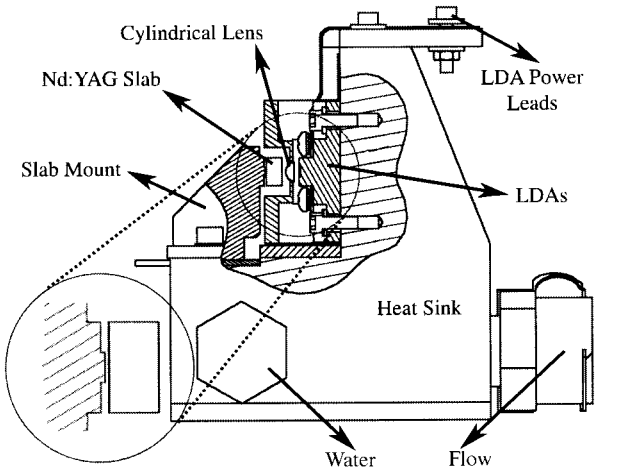

Fig. 5. End view of the HELT pump head. This version shows an integrated water path at the base, but the present design is clamped to a water-cooled plate to better simulate conductive cooling for the complete assembly. Note the stepped slab mounting surface in detail.

5. Step Mount

Computer modeling of the laser head assembly, which included the thermal extraction capability, helped determine the steady-state thermal characteristics of the slab. This modeling indicated that conductive cooling from the HR-coated side of the slab resulted in the smoothest set of thermal gradients compared with cooling the slab from the two uncoated sides. From these calculated isotherms, a thermal lens model was created to predict the lens strengths that produced results near the measured values. Furthermore, thermal modeling of the back-mounted slab shows that the isotherms can be given a less-severe curvature if the thermal conductivity directly behind the diode-pump path is higher than on either side. To accomplish this, we machined a 0.230-mm tall center step along the slab heat sink length (see expanded view in Fig. 5). The step has a single layer of thermally conductive bonding tape on either side of the center and a single layer across the whole bonding width. Figure 6 shows the calculated isotherms for the flat-surface slab mount and the step surface, respectively. These results are for pumping with an average power of 31 W and a 0.36 heating fraction, which is defined as the fraction of pump power going into heat. The optical power deposition in the slab assumes a Beer's Law absorption of pump light marked by the two vertical lines on each side of the center. The top center of the slab was found to have a slightly higher temperature at the top of the slab in the step-mounted case (~1 °C), but the curvature of the isotherms was diminished, indicating a weaker thermal lens in the slab. The steady-state focal length was reduced from ~40 cm with the flat mount to ~65 cm with the step mount. This lensing was then compensated by the use of an intracavity negative cylindrical lens, shown in Fig. 1.

To simulate any future use of such a pump head design in a space-based conductively cooled laser system, we mounted the unit to a water-cooled plate for heat removal. Here, the diode-array wavelength selection contributed significantly toward final system performance. A small reduction in peak thermal lensing and temperature sensitivity as well as a small decline in total system efficiency were the results of choosing diode arrays with a significant wavelength spread (±3.5 nm) around 809 nm.

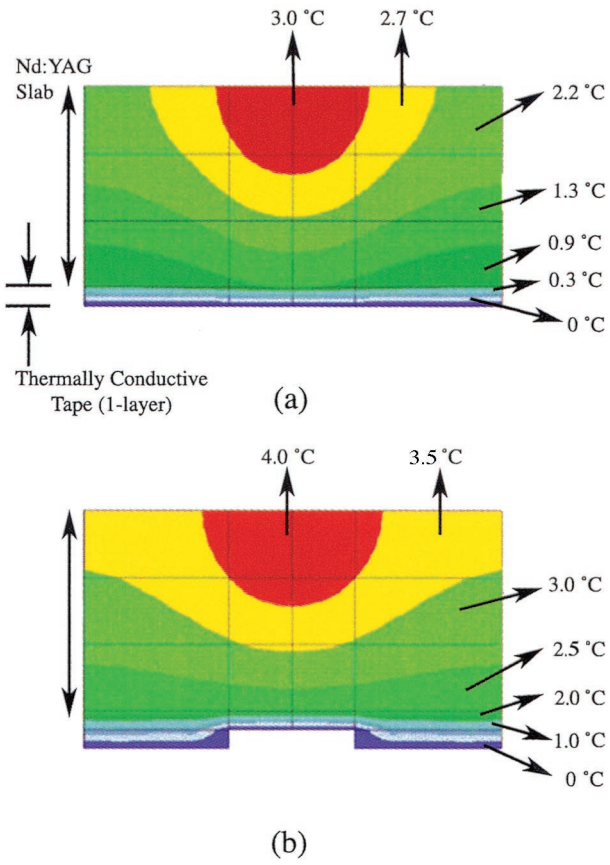

Fig. 6. (a) Calculated thermal distribution in the Nd:YAG cross section. The borders between shaded areas represent isotherms. This slab was modeled with a flat heat-sink interface. (b) Calculated thermal distribution in slab but with a stepped thermal interface. The introduction of a double layer of thermal conductive tape on the sides of the central region helps reduce the effective thermal lens.

6. Unstable Resonator

An unstable resonator has the capability of creating a relative large beam in a modest geometrical cavity length. When the resonator is coupled with a GRM, near-TEM_{oo} output can be achieved. The most important feature of an unstable resonator is its magnification M. Magnification directly affects the dissipative losses (feedback), higher-order mode discrimination, alignment sensitivity, and the GRM spot size relative to the beam waist in the active media.[13–15] There are a variety of decisions to be made in arriving at a cavity design and its magnification. The unstable resonator was designed in consultation with M. Morin of the National Optics

Institute of Canada.[16] The Institute also produced the graded reflectivity output coupler.

The final empty cavity design employed a geometrical length of 41 cm with a convex output coupler (GRM) radius of −237 cm and a concave HR reflector of radius +300 cm. This provided a total magnification (geometrical plus diffraction) of $M_t = 1.4$. A Gaussian GRM profile was chosen with an intensity reflectivity profile of $R(r) = R_o \exp[-2(r/\omega_m)^2]$, where R_o is the reflectivity in the mirror's center and ω_m is the $1/e^2$ radius of the profile. To sweep the most energy out of the gain medium, we designed the GRM for a beam waist in the Nd:YAG slab of ~1.1 mm. The relationship between ω_i (the beam waist at the output coupler) and the reflective Gaussian profile waist on the mirror was $\omega_i = \omega_m(M^2 - 1)^{1/2}$. Requiring $\omega_i = 1.1$ mm gave a Gaussian reflective waist of $\omega_m = 1.12$ mm.

Much of unstable resonator design can be reasoned through use of the geometrical approximation of Siegman.[13] By use of the g_i values associated with the resonator, $g_i = 1 - L/R_i$, the geometrical magnification can be shown to be

$$M_g = G + (G^2 - 1)^2, \tag{2}$$

where $G = 2g_1 \cong g_2 - 1$ and is equal to 1.265 for our resonator. As mentioned above, the complete theoretical calculation gave a magnification of 1.4, which showed the effects of diffraction and the limitation of the geometrical approximation in our case. The mode discrimination between the fundamental mode ω_o and higher-order modes ω_n was

$$\omega_n = \omega_o/(M)^{2n}, \tag{3}$$

thus high magnification was desirable. Unfortunately, very high values of magnification give rise to higher losses that cannot be overcome in most applications. Substituting 1.4 for the magnification in Eq. (3) indicates we had a factor-of-2 discrimination between the fundamental and the next-highest mode. The GRM further aided in discrimination against higher-order modes.

Feedback for the first-order mode has been shown to be $\langle R \rangle = R_o/M^2$. Our requirements were for an effective output-coupler feedback of ~0.32. This result was based on a plane-wave analysis that included the gain and dissipative losses expected in the physical cavity design.[17,18] To achieve an effective reflectivity of $\langle R \rangle \sim 0.32$, we required a Gaussian center reflectivity of $R_o \sim 63\%$ for $M = 1.4$.

Another important consideration is the cavity alignment stability. Krupke and Sooy[19] showed that the angular alignment sensitivity S can be expressed as

$$S = (1 - g_2)/(1 - g_1). \tag{4}$$

Smaller values of this parameter are desirable. By definition, unstable resonators have values of g_1g_2 either greater than 1 or less than 0. For positive branch resonators, which apply in our case, the value of g_1g_2 is not far from unity. It is another design trade-off to arrive at a resonator that has a relatively low S and a reasonable magnification. For our cavity, the design sensitivity value of $S \sim 10$. This can be compared to a value of $S \sim 3$ for a very stable resonator with $g_1g_2 \sim 0.5$.

7. Experimental Procedure to Optimize the Laser

The thermal lens created in the slab was a function of average pump power and lasing efficiency. The laser was optimized at a single pump power for which the intracavity negative cylindrical lens best compensated the positive thermal lens in the slab. The slab lens changed strength as the laser achieved steady-state performance, owing to the effect of stimulated emission cooling; this effect was readily seen in the CCD array beam analysis. To understand the effects of various cylindrical lenses on the cavity oscillator performance, we measured the spot sizes on the HR and the GRM using $2f$ imaging systems in addition to the far-field pattern. The beam waists on the HR and GRM were compared to results produced by PARAXIA modeling of the resonator.[20] This comparison allowed us to determine the effective strength of the thermal lens under operation, and helped us to fine tune the final operation of the laser.

We initially fired the laser in quasi-cw mode. If the thermally compensating cylindrical lens is too negative, output power was low and the imaged beam spots on the mirrors were large relative to the design radius ~1 mm. The cylindrical lens was then made less negative until the design spot size was obtained. Next, the laser was Q switched, and small adjustments made until the far-field pattern was nearly Gaussian in both axes. It was an interesting feature of the unstable resonator that the Q-switched power was significantly *greater* than that found in the long-pulse mode. This, of course, is not the case in stable cavity resonators. Typically, our unstable-cavity Q-switched pulse energy was greater than that produced in long-pulse mode by about 25%–30%. This was due to the high losses attendant to the unstable resonator, which affect the inversion negatively when lasing in quasi-cw.

8. Lifetime Study and Summary of Results

A. Lifetime Study

After completing its initial configuration tests, HELT was put through a simulation of the laser requirements over the two-year VCL mission. VCL output specifications required the laser to fire 2.4×10^9 shots at a pulse energy of 10–15 mJ over a one-year period.[1] In the simulation of the second year, the pump pulse width would be increased to regain lost pump energy due to diode-array degradation. Additionally, the beam quality was required to maintain ≤2.7 mm mrad, or ≤2 times the diffraction limit.

B. Setup

Figure 7 shows the configuration of the lab and data acquisition system. The test facility was employed

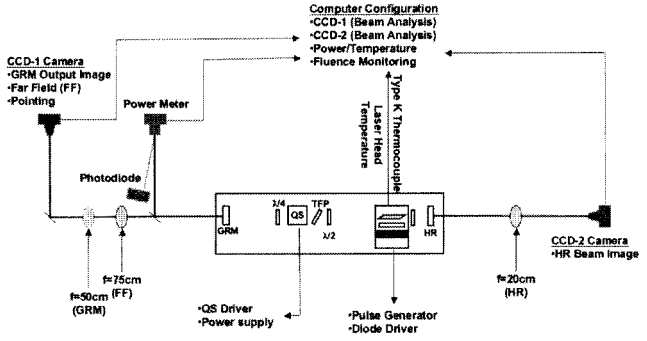

Fig. 7. HELT life test configuration. Intracavity beam profiles were monitored to track the fluences in the slab.

for measuring the laser's short- and long-term performance. The life test was semiautomated, and performance parameters such as pulse energy, temperatures, and far-field (FF) divergence were recorded. We paid particular attention to beam sizes on the HR mirror in order to keep an accurate real-time account of the intracavity fluence. The HR mirror's proximity to the slab provided a more accurate measure of the fluence near the slab, the most damage-sensitive optic in the cavity. From head assembly experiments discussed earlier, we determined that it was important to avoid going over a intracavity fluence 3 J/cm^2 to avoid optical damage. Long-term pointing stability was not an important factor for this experiment, since most of the components were held in unlockable commercial gimbal mounts and translation stages for alignment sensitivity experiments. If a flight unit is to be built, further long-term testing will be required for pointing and other parameters relevant to the particular mission selected.

C. Data and Measurements

Figure 8 shows the results of the 4.8×10^9 shot lifetime test. The first 2.4×10^9 shots show a steady decay in the output energy from 15 to 10 mJ as expected owing to diode degradation. Laser slab surface inspections were performed at regular intervals

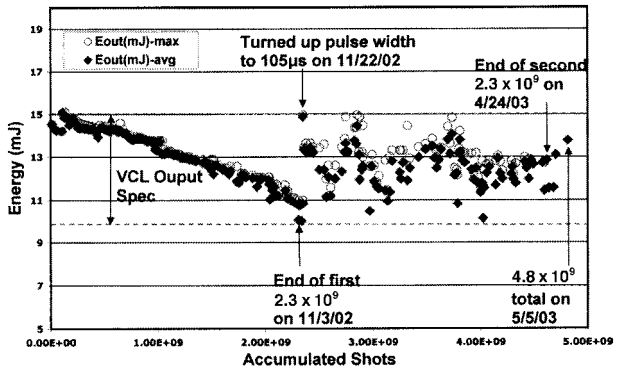

Fig. 8. Average power output lifetime data. At 2.3×10^9 shots, the diode current pulse was increased to 100 μs to accommodate the degradation in diode output. The erratic behavior for the second 2.3×10^9 shots was due to several power outages, water chiller problems, and diode driver failure. However, even with these added stresses, no damage was present after 4.8×10^9 shots.

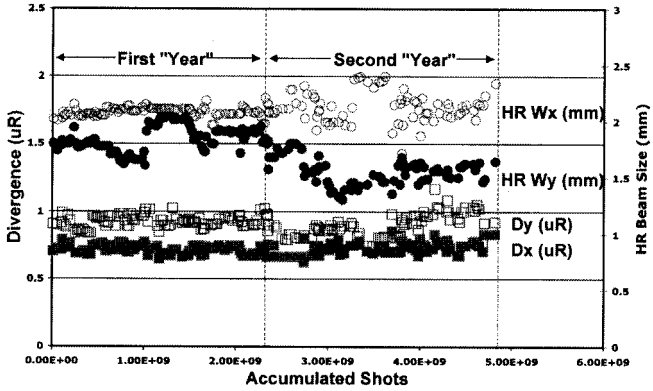

Fig. 9. Lifetime data of the intracavity beam diameter on the HR mirror and the far-field divergence.

to verify that no microscopic damage was present, which would cause premature performance decay and could eventually contribute to a catastrophic failure of other cavity optics. After 2.4×10^9 shots, there was no damage found in any of the cavity optics, but inspection of the diodes revealed that a single bar was lost on one array. After slab reinstallation and minor realignment, the pump pulse length was increased from 89 to 105 μs to restore the output energy to 15 mJ. This roughly simulated the procedure that would be performed in space in order to maintain an altimetry link. Over the following months, new chillers and flow switches installed for second-year operation had difficulties keeping the laser head at the set temperature, which often triggered the safety interlocks and caused hard shutdowns of the laser. When the numerous building power outages, humidity cycles, and lab-temperature swings over the winter season were factored in the laser environment, a harsher life test was actually performed than otherwise planned. The final result was that after more than 4.8×10^9 10–15 mJ laser pulses, there was no optical damage present in the system.

It was also important to be sure that acceptable beam quality was maintained over the test period. The beam quality data is summarized in Fig. 9. The typical $1/e^2$ FF divergence measurement averaged 0.87 ± 0.05 mR in the x axis and 1.10 ± 0.08 mR in the y axis. The beam sizes on the HR, despite some fluctuations in the second year owing to the previously mentioned environmental problems, averaged 1.75 ± 0.08 mm and 1.43 ± 0.15 mm for the x and y axes, respectively. Examples of FF and HR beam images are shown in Figs. 10(a) and 10(b), respectively. Typical external GRM diameters throughout the life test were $2.00 \text{ mm} \pm 0.14 \times 2.14 \text{ mm} \pm 0.29$ mm in the x and y axes, respectively. From the GRM data and FF divergences, we are able to approximate the M^2 values for the full 4.8×10^9 shots as $M_x^2 = 1.29 \pm 0.15$ and $M_y^2 = 1.74 \pm 0.31$.

D. Fluence and Efficiency

During the first half of the test, the fluence stayed below 3 J/cm^2, but in the second year of operation it

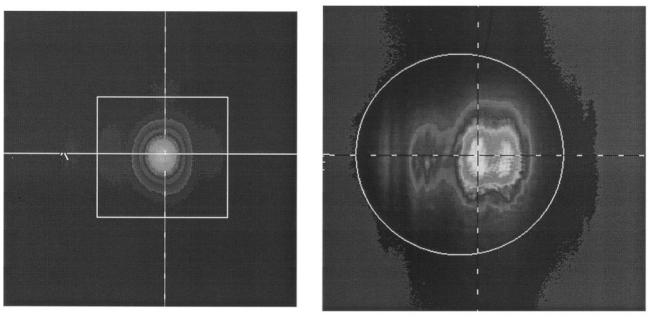

(a) (b)

Fig. 10. (a) Typical HELT far-field output pattern as formed at the focal plane of a $f = 75$ cm positive lens. (b) HELT intracavity beam image on the HR mirror. This was captured regularly with the other pertinent lifetime data to monitor the fluence in the cavity.

regularly surpassed that mark owing to the aforementioned environmental problems. Maximum fluences were calculated by using $F = E/A_{\mathrm{AVG}}$, with $A_{\mathrm{AVG}} = \pi(D_X D_Y)/8$ and $E = [(R + 1)/(1 - R)]E_{\mathrm{OUT}}$. D_X and D_Y are the $1/e^2$ beam diameters on the HR mirror, and R is the average reflectivity of the GRM as defined in the unstable resonator section. The quantities E and E_{OUT} are the energies inside and outside the cavity, respectively. The peak optical efficiency at the beginning of the first year was 12.5% and fell to 10.4% at the start of the second year. These efficiencies are lower than the design values for the laser owing to running the pump diodes at de-rated current and the fact that the diodes had been used for many untabulated hours during the laser development before the lifetime study.

9. Conclusions

Extensive work has been performed on a standard side-pumped zigzag slab head design such that with some minor, yet essential, changes, maximum efficiency and good single spatial mode operation were achieved without an intracavity aperture in an unstable resonator design. A long-term operational test was performed for over 4.8×10^9 pulses in a relatively unclean and uncontrolled laboratory environment to help prove its reliability and resistance to optical damage. An upper limit of allowed intracavity fluence has been measured experimentally as $\leq 3\ \mathrm{J/cm^2}$. How this data can be applied to other similar unstable resonator designs of varying powers is not conclusive, but work is under way to help determine the extent. Further work is planned with new diode arrays to determine experimentally and theoretically the design's limits in average output power, pulse energy, and repetition rate. A test is planned to determine how HELT performs under vacuum and what, if any, changes may be required in the design.

This work was supported in part by National Aeronautics and Space Administration Cooperative Research Agreements NCC 5-269, NCC 5-482 and NCC 5-630 with the Laser Physics Group, Department of Physics, American University, Washington, D.C.

References and Note

1. D. B. Coyle, R. B. Kay, and S. J. Lindauer, "Design and performance of the vegetation canopy lidar (VCL) laser transmitter," in *Aerospace Conference Proceedings* (Institute of Electrical and Electronics Engineers, New York, 2002), Vol. 3, pp. 1457–1464.
2. J. B. Abshire, J. C. Smith, and B. E. Schutz, "Geoscience Laser Altimeter System (GLAS)," in *17th International Laser Radar Conference* (Sendi, Japan, 1994); see also http://glas.gsfc.nasa.gov/.
3. J. B. Blair and M. A. Hofton, "Modeling laser altimeter return waveforms over complex vegetation using high-resolution elevation data," Geophys. Res. Lett. **26,** 2509–2512 (1999).
4. T. J. Kane, R. C. Eckardt, and R. L. Byer, "Reduced thermal focusing and birefringence in zig-zag slab geometry crystalline lasers," IEEE J. Quantum Electron. **19,** 1351–1354 (1983).
5. J. M. Eggleston, T. J. Kane, K. Kuhn, J. Unternahrer, and R. L. Byer, "The slab geometry laser-part I: theory," IEEE J. Quantum Electron. **20,** 289–301 (1984).
6. E. Armandillo, C. Norrie, A. Cosentino, P. Laporta, P. Wazen, and P. Maine, "Diode-pumped high efficiency high-brightness *Q*-switched Nd:YAG slab laser," Opt. Lett. **22,** 1168–1170 (1997).
7. R. S. Afzal, "Mars observer laser altimeter-laser transmitter," App. Opt. **33,** 3184–3188 (1994).
8. R. S. Afzal, A. W. Yu, J. J. Zayhowski, and T. Y. Fan, "Single-mode high-peak-power passively *Q*-switched diode-pumped Nd:YAG laser," Opt. Lett. **22,** 1314–1316 (1997).
9. D. B. Coyle, "Injection seeded, diode-pumped, short pulse Nd:YAG ring laser for space based laser ranging," Ph.d. Dissertation (American University, Washington, D.C., 1992).
10. T. Y. Fan and R. L. Byer, "Diode laser-pumped solid state lasers," IEEE J. Quantum Electron. **24,** 895–912 (1988).
11. W. Koechner, *Solid-State Laser Engineering* (Springer, New York, 1999).
12. B. Zhou, T. J. Kane, G. J. Dixon, and R. L. Byer, "Efficient, frequency-stable laser-diode-pumped Nd:YAG laser," Opt. Lett. **10,** 62–64 (1985).
13. A. E. Siegman, "Unstable optical resonators for laser applications," Proc. IEEE **53,** 277–287 (1965).
14. S. De Silvestri, P. Laporta, M. Magni, and O. Svelto, "Solid-state laser unstable resonators with tapered reflectivity mirrors: the super-Gaussian approach," IEEE J. Quantum Electron. **24,** 1172–1177 (1988).
15. M. Morin, "Graded reflectivity mirror unstable laser resonators," Opt. Quantum Electron. **29,** 819–866 (1997).
16. M. Morin, National Optics Institute, 369 Franquet, Saint-Foy, Quebec, Canada G1P 4N8, (personal communication, 1998).
17. J. J. Degnan, "Theory of the optimally coupled *Q*-switched laser," IEEE J. Quantum Electron. **25,** 214–220 (1989).
18. D. B. Coyle, D. V. Guerra, and R. B. Kay, "An interactive numerical model of diode-pumped, *Q*-switched/cavity dumped lasers," J. Appl. Phys. **28,** 452–462 (1995).
19. W. F. Krupke and W. R. Sooy, "Properties of an unstable confocal resonator CO_2 laser system," IEEE J. Quantum Electron. **5,** 575–86 (1969).
20. PARAXIA is a general laser beam propagation and laser resonator analysis program. See http://www.sciopt.com.